# Space Weather
# Lecture 3: Bow Shock

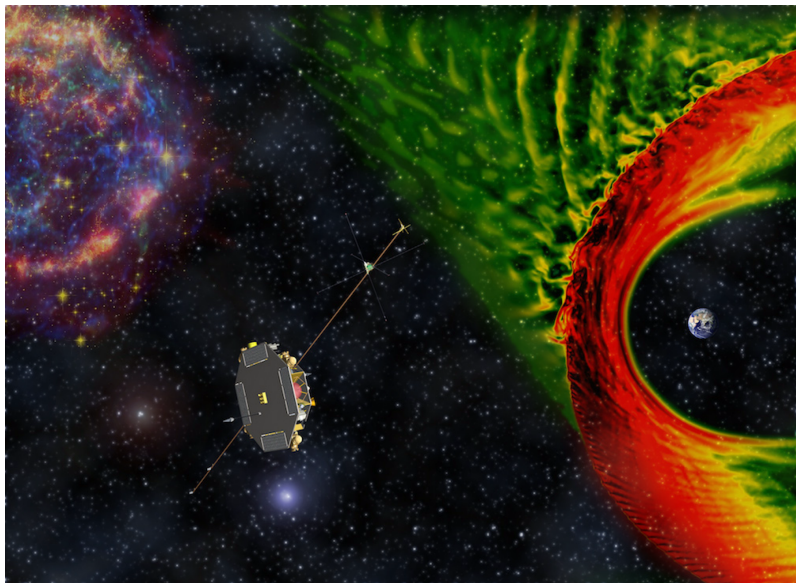

Elena Kronberg (room 442)
elena.kronberg@lmu.de

# Introduction: Shock wave

A disturbance that travels faster than the local sound speed (or, in general, a characteristic wave speed) is a *shock wave*.

Sn 1006 brightest supernovae ever

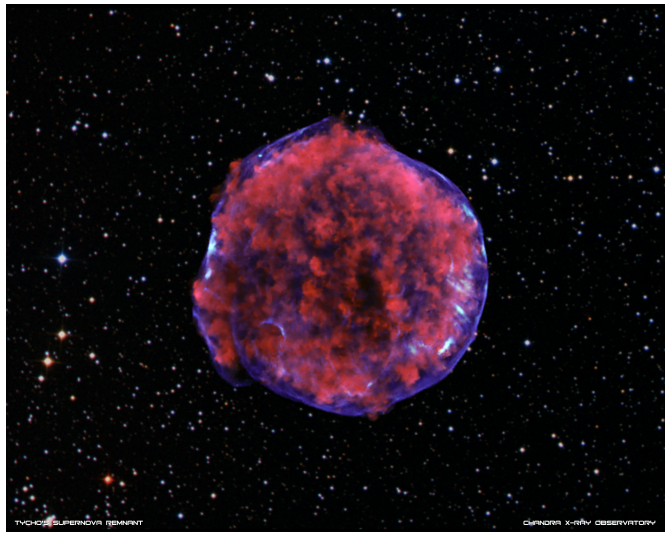

X-43 fastest aircraft


Tail of diplodocus exceeded speed of sound, ~1200 km/h

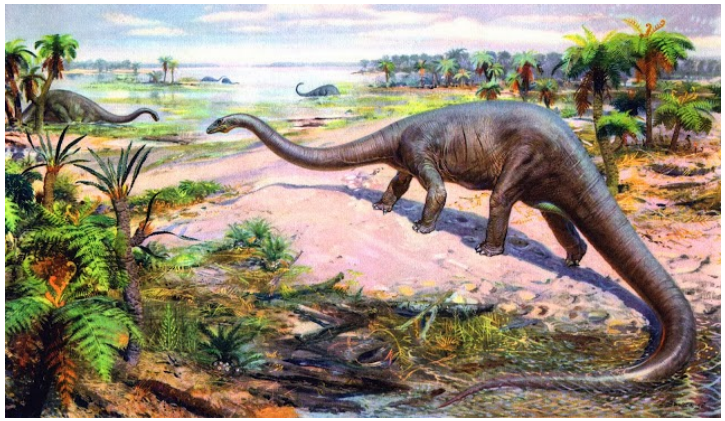

Pistol shrimp, kills enemies at distance by releasing a sound reaching 218 decibels

# Introduction: Sound and Alfvén speeds

- The *sound speed* is

$$c_s = (\gamma p/\rho)^{1/2},$$

where $\gamma$ is the ratio of specific heat, $p$ is the gas pressure and $\rho$ is the mass density. This is the characteristic speed at which information is transmitted through non-ionized, non-magnetic gases.

- The *Alfvén speed* is

$$V_A = \frac{B}{\sqrt{\mu_0 \rho}}.$$

This is the characteristic speed at which information is transmitted along a magnetic field in a plasma.

# Introduction: Slow and fast magnetosonic speed (ms)

The MHD equations yield several types of waves:

$$c^2_{\mathrm{ms\,slow}} = \frac{1}{2}\left[\left(c_s^2 + V_A^2\right) - \sqrt{\left(c_s^2 + V_A^2\right)^2 - 4c_s^2 V_A^2 \cos^2\theta_{Bn}}\right],$$

$$c^2_{\mathrm{ms\,fast}} = \frac{1}{2}\left[\left(c_s^2 + V_A^2\right) + \sqrt{\left(c_s^2 + V_A^2\right)^2 - 4c_s^2 V_A^2 \cos^2\theta_{Bn}}\right],$$

where $\theta_{Bn}$ is the angle between the incoming magnetic field and the shock normal vector.

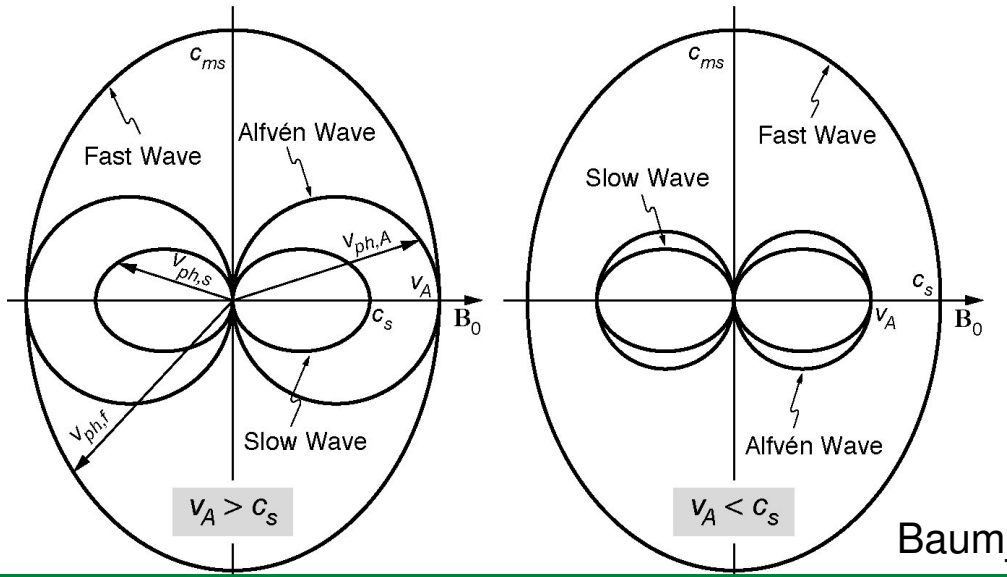


Baumjohann&Treumann 1996

# Introduction: Mach numbers

- Sonic Mach number is

$$M_{\mathrm{s}} = \frac{v}{c_{\mathrm{s}}},$$

  where $v$ is fluid velocity.

- Slow Magnetosonic Mach number is

$$M_{\mathrm{ms\,slow}} = \frac{v}{c_{\mathrm{ms\,slow}}}$$

- Alfvén Mach number is

$$M_{\mathrm{A}} = \frac{v}{V_{\mathrm{A}}}$$

- Fast Magnetosonic Mach number is

$$M_{\mathrm{ms\,fast}} = \frac{v}{c_{\mathrm{ms\,fast}}}$$

# Introduction: Shock

*Shocks* are transition layers where the plasma properties change from one equilibrium state to another.
The relation between the plasma properties on both sides of a shock can be obtained from the conservative form of the MHD equations, assuming conservation of mass, momentum, energy, $\partial B/\partial t = \nabla \times (v \times B)$ and of $\nabla \cdot \mathbf{B} = 0$.

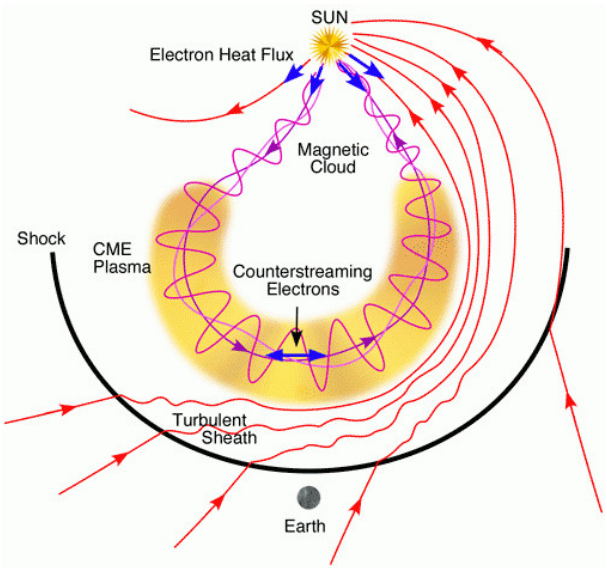


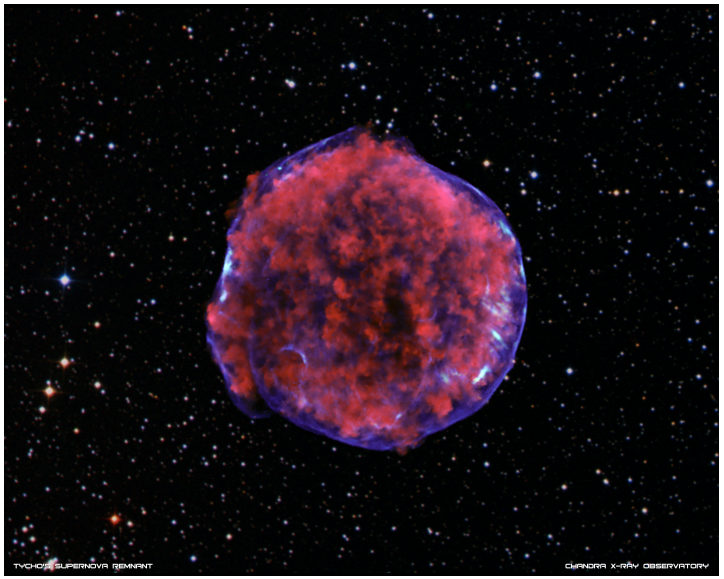

# Shock-Conservation Relations

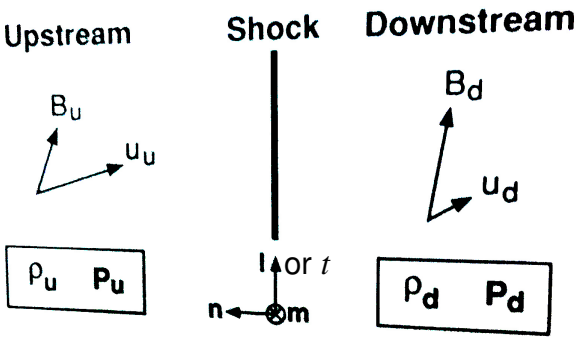


- The jump across the shock in any quantity $X$:

$$[X] = X_u - X_d$$

- For any quantity, a conservation equation is

$$\frac{\partial Q}{\partial t} + \nabla \cdot F = 0,$$

where $Q$ and $F$ are the density and flux of any conserved quantity. If shock is steady and one-dimensional (variations only along $n$-axis), then

$$\frac{\partial F_n}{\partial n} = 0.$$

The component of the conserved flux normal to the shock is constant

$$[F_n] = 0.$$

For MHD, the conservation of mass in one dimesion is $\frac{\partial \rho v_n}{\partial n} = 0$ which leads to the jump condition for the shock: $[\rho v_n] = 0$.

# Rankine-Hugoniot jump conditions for ideal MHD

$$[B_n]_u^d = 0 \tag{1}$$

$$[v_n B_t - v_t B_n]_u^d = 0 \tag{2}$$

$$[\rho v_n]_u^d = 0 \tag{3}$$

$$[\rho v_n^2 + p + B_t^2/2\mu_0]_u^d = 0 \tag{4}$$

$$[\rho v_n v_t - B_n B_t/\mu_0]_u^d = 0 \tag{5}$$

$$\Big[\frac{1}{2}\rho v^2 v_n + \frac{\gamma}{\gamma-1}\rho v_n + \frac{B_t(v_n B_t - v_t B_n)}{\mu_0}\Big]_u^d = 0 \tag{6}$$

# Fast Shocks: $M_{\mathrm{ms\,fast}} > 1$

- Plasma pressure and field strength (Alfvén speed) increase downstream of shock; magnetic field bends away from normal
- Fast shocks are by far the most frequent types of shocks observed in solar-system plasmas (Earth's bow shock. . . )

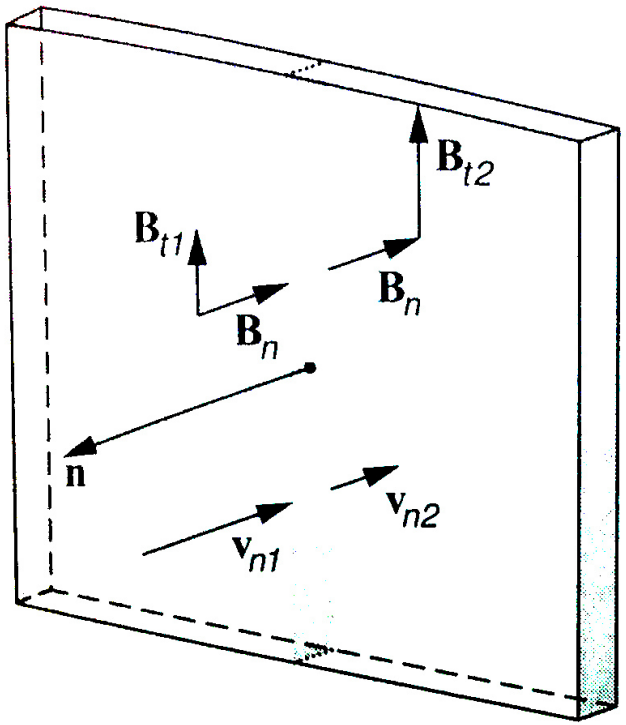


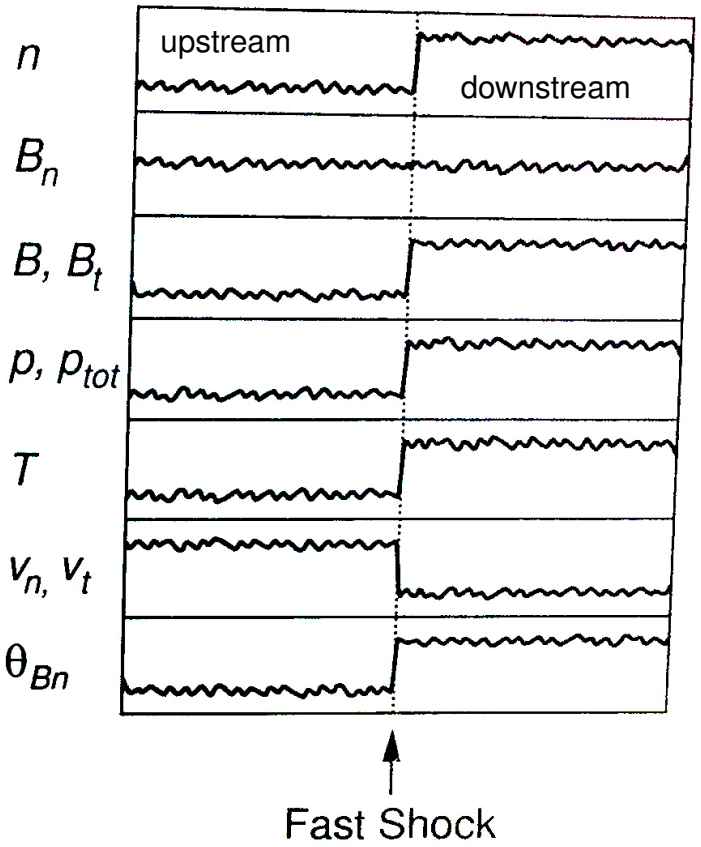

# Bow Shock: definition

- The most famous example of a plasma shock is the Earth's bow shock.
- It develops as a result of the interaction of the Earth's magnetosphere with the supersonic solar wind.
- When $M_{ms} > 1$ and the plasma flow is distorted by a stationary object, a shock front develops, across which fluid quantities jump discontinuously.
- The super-magnetosonic flow will become sub-magnetosonic.

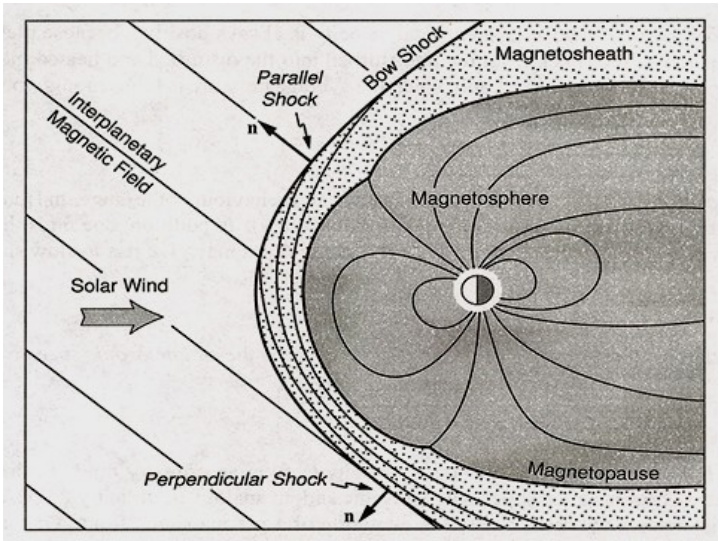

# Bow Shock: characteristics

- The surface of the bow shock is parabolically shaped, $M_{ms} \simeq 8$.
- Mach number is defined by the solar wind velocity component normal to the shock, $v_n = v_{sw} \cos\theta$. The condition $M_{ms} > 1$ is satisfied when $\theta < \arccos M_{ms}^{-1}$. Therefore, bow shock forms at $\theta_{max} \simeq 80°$.
- Bow shock divides the solar wind flow into two regions: the undisturbed region upstream of the bow shock and the disturbed magnetosheath flow on the downstream side.

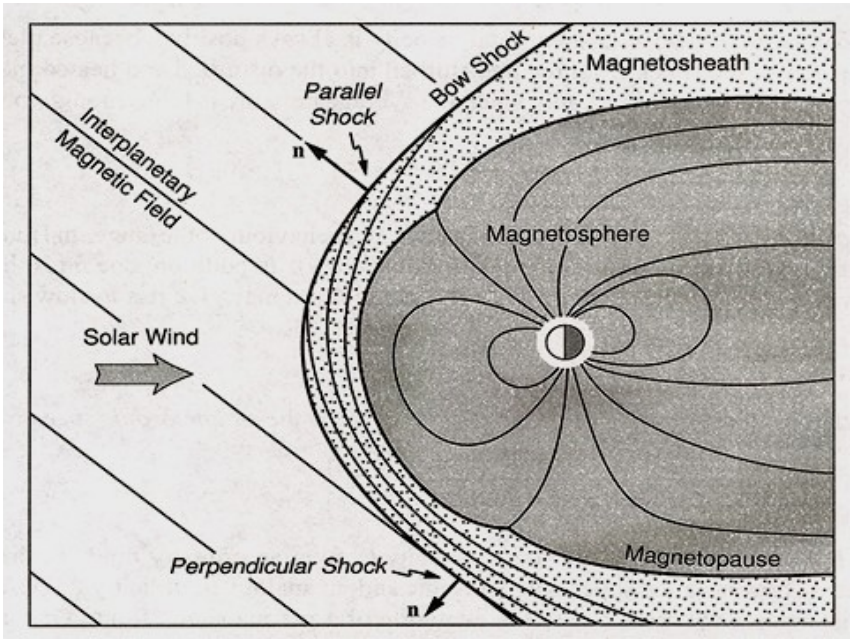

# Shape of the bow shock: Mach cone

- In case $V_A \gg c_s$, the Alfvén Mach cone angle defines the shape

$$\theta_A = \arcsin\left(\frac{V_A}{v_{sw}}\right) = \arcsin M_A^{-1}$$


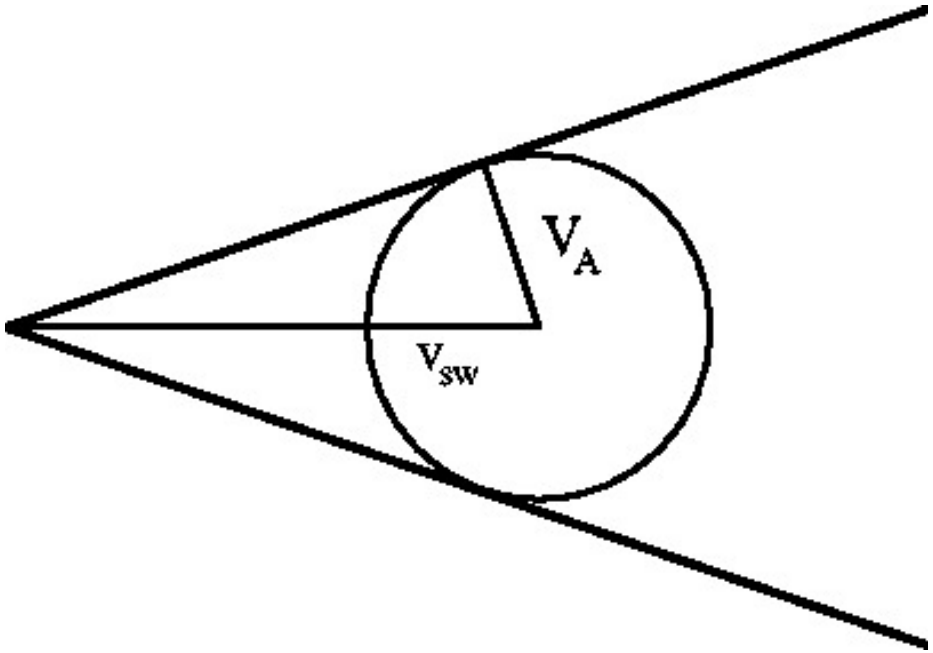


$M_A$ =9.7 (lowest curve) . . . 1.4 (highest curve)

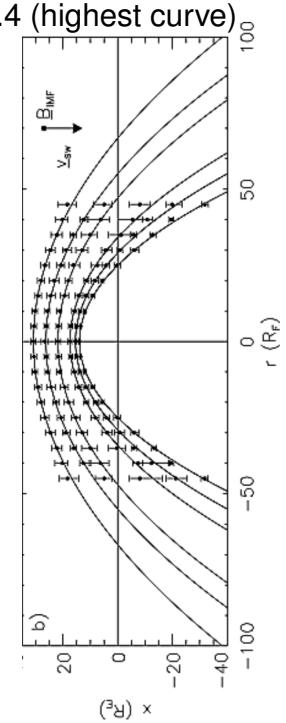


Chapman and Cairns, 2003

# Position of the bow shock and magnetosheath

- The position of the bow shock highly varies depending on solar wind dynamic pressure, IMF and $M_A$ (e.g. model by Peredo+95).

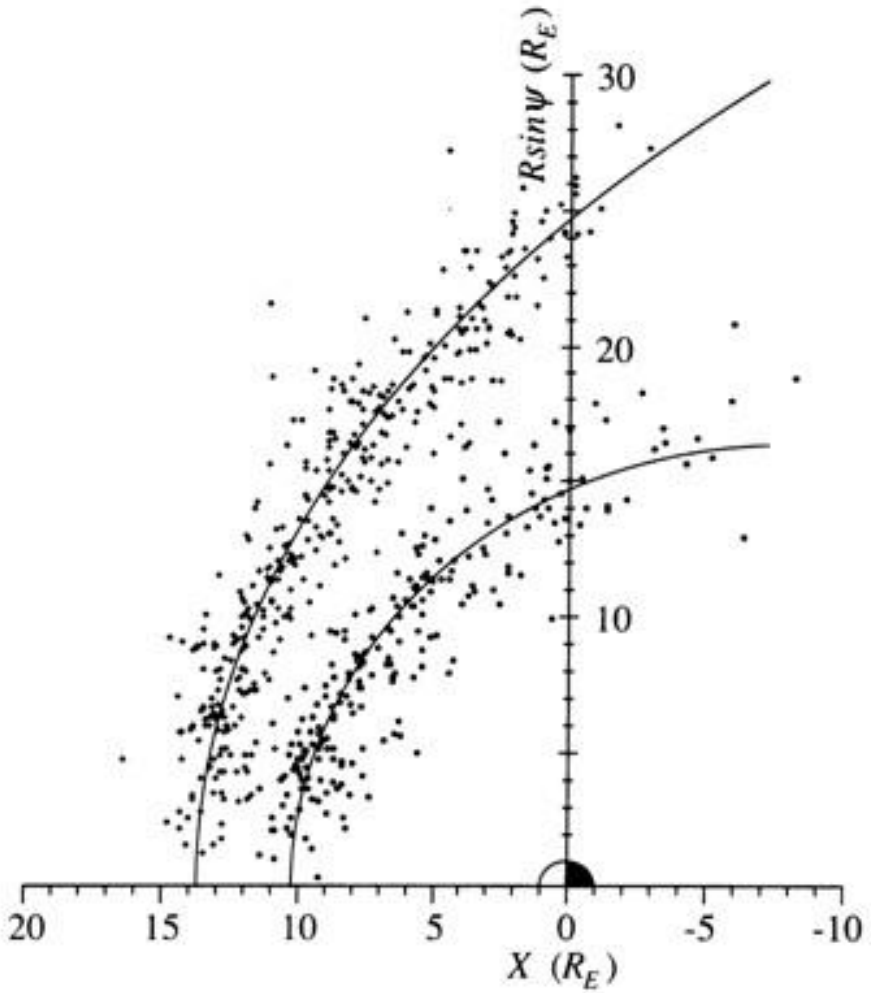

# Formation of the bow shock

Vlasiator simulations: Plasma density, IMF at 30°

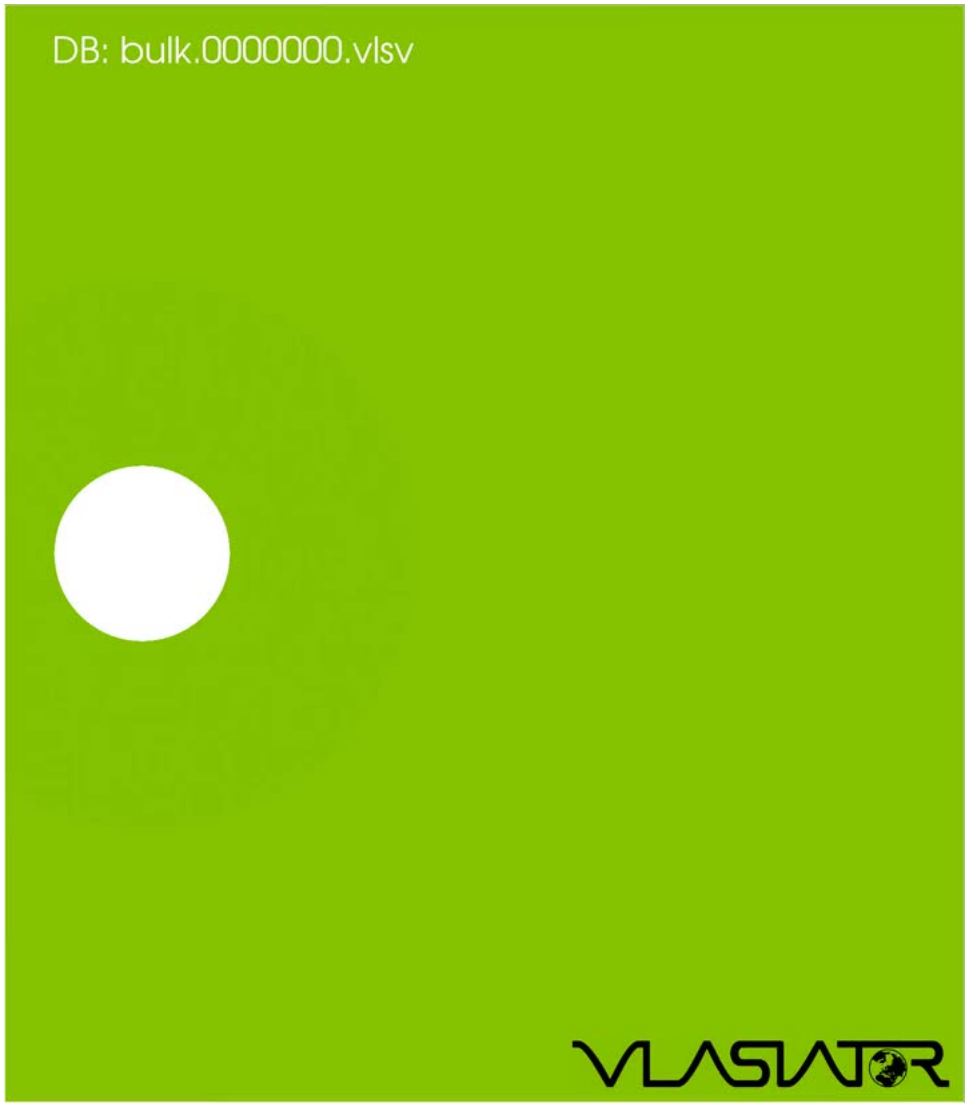

# Formation of the bow shock

Vlasiator simulations: Magnetic field magnitude, IMF at 5°

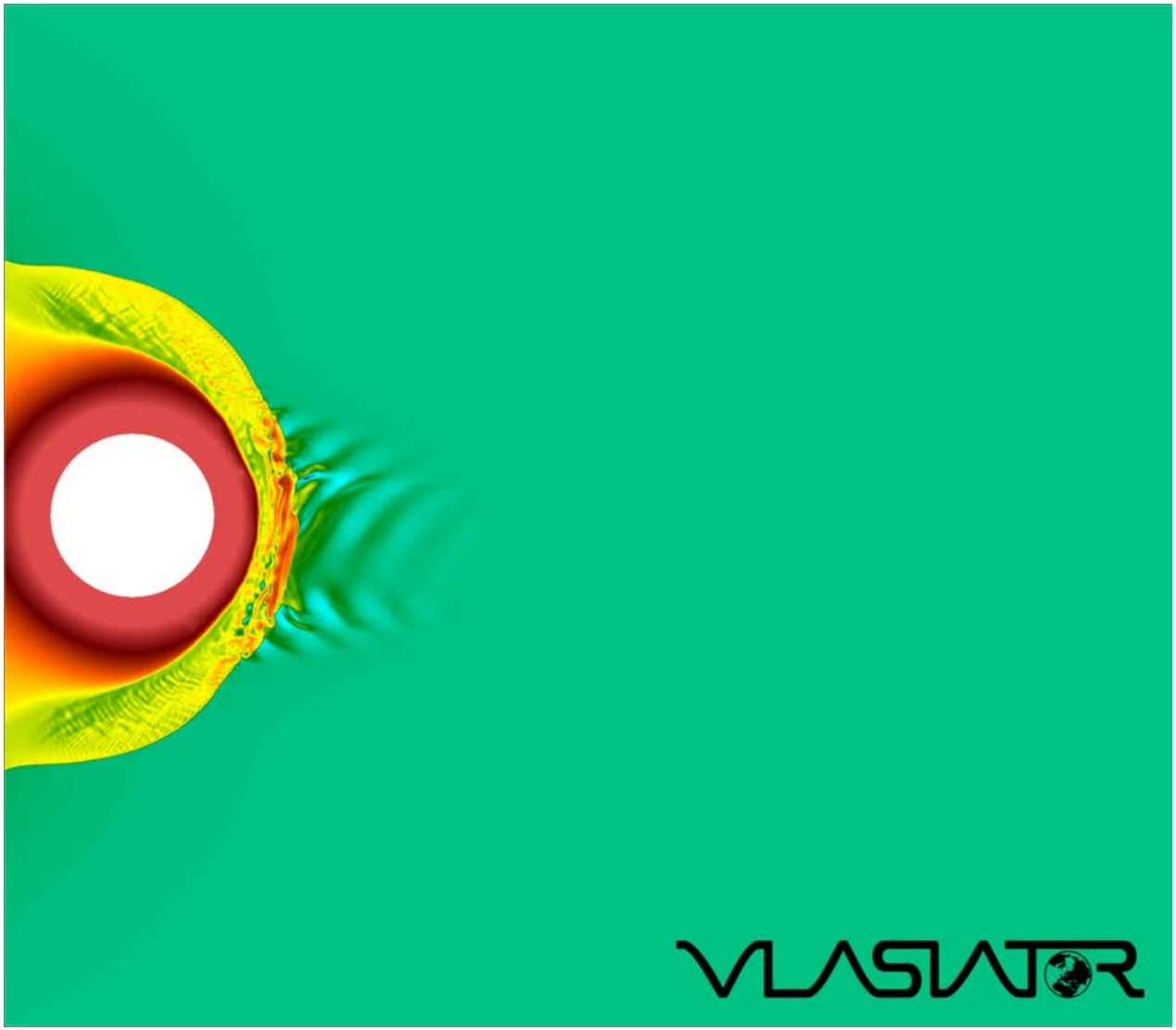

# Slow shocks: $M_{\mathrm{ms\,slow}} > 1$

- Plasma pressure increases; magnetic field strength (Alfvén speed) decreases; magnetic field bends toward normal

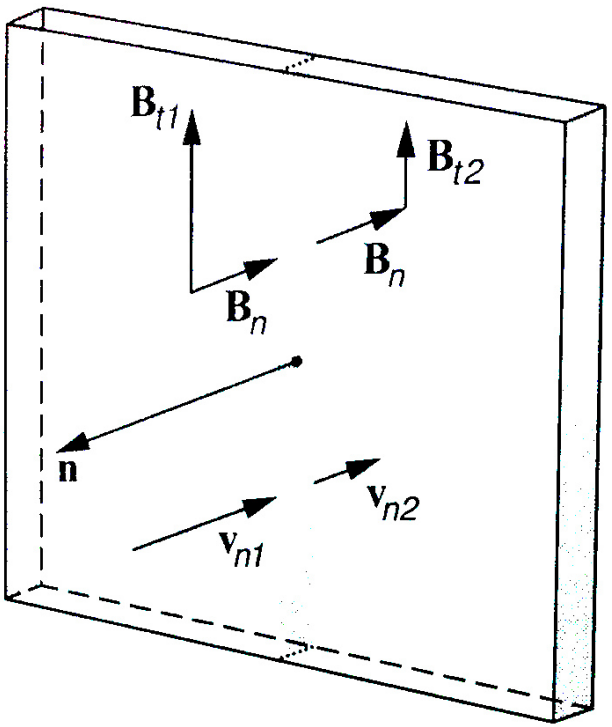


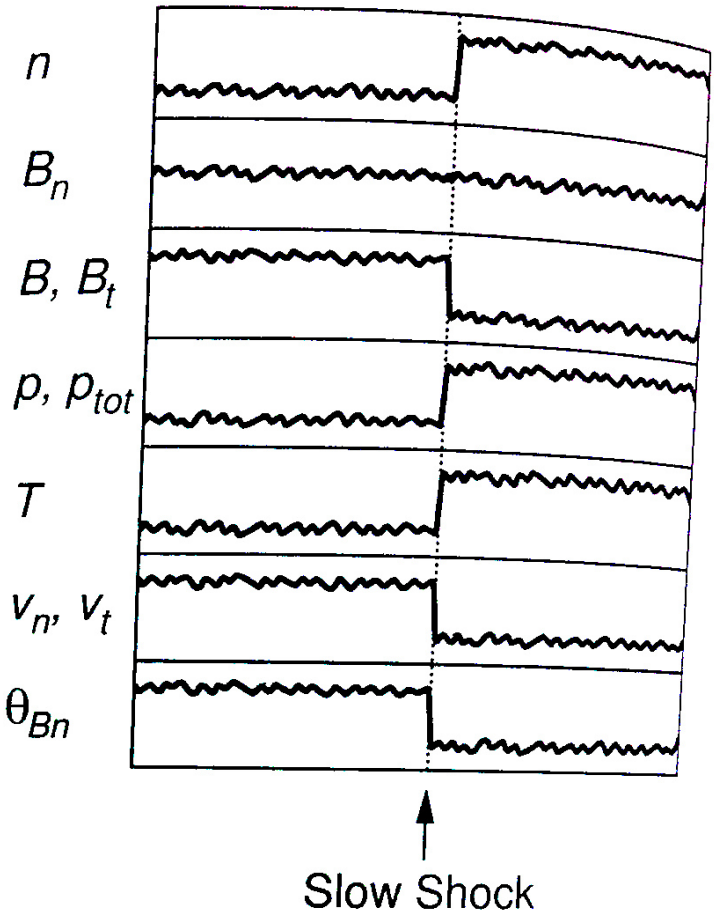

# Slow shocks

Petscheck magnetic reconnection is associated with a slow-mode shock; can be related to magnetic reconnection in the solar corona.

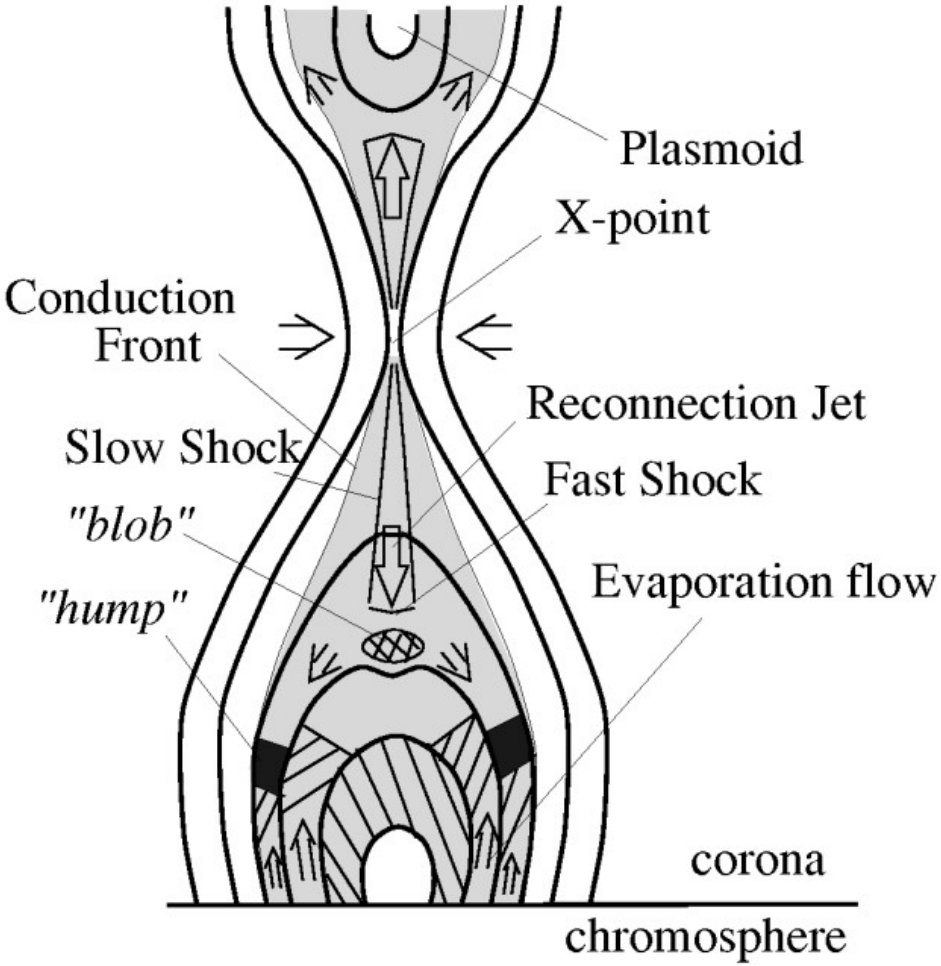

# Parallel and perpendicular shocks

- Strictly in parallel shocks the magnetic field is not affected by the shock.
- Realistic parallel shocks are always quasi-parallel and therefore affect the magnetic field amplitude.
- The shock becomes turbulent.

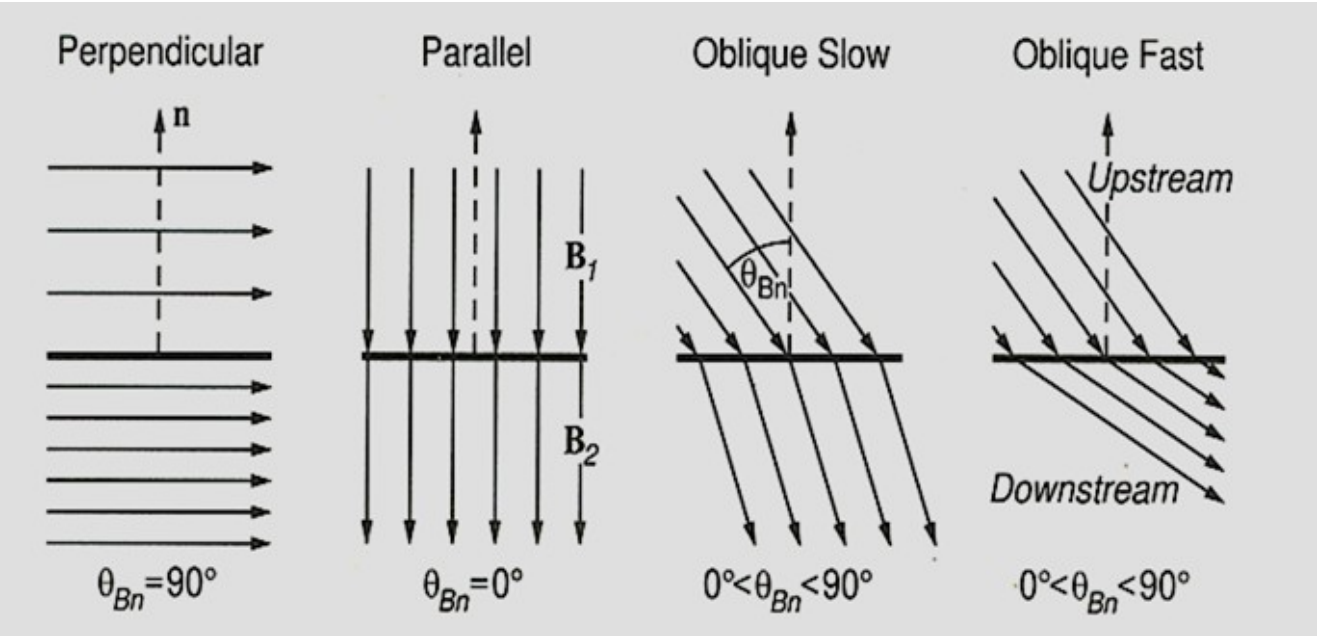

# Parallel and perpendicular shocks

- Typical magnetic shock profiles

The field has a sharp jump called the ramp preceded by a gradual rise called the foot. The field right behind the shock is higher than its eventual downstream value. This is called the overshoot.

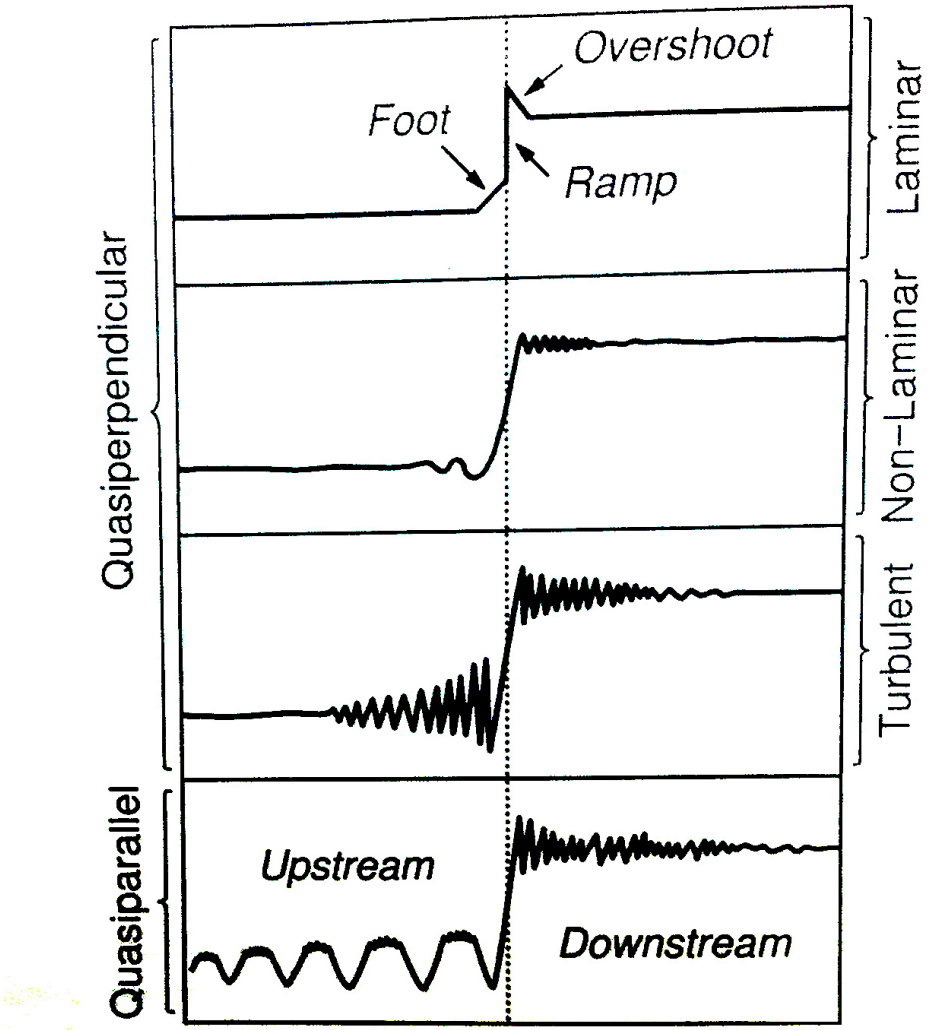


A laminar fluid flows in parallel layers, with no disruption between the layers

# Parallel and perpendicular shocks

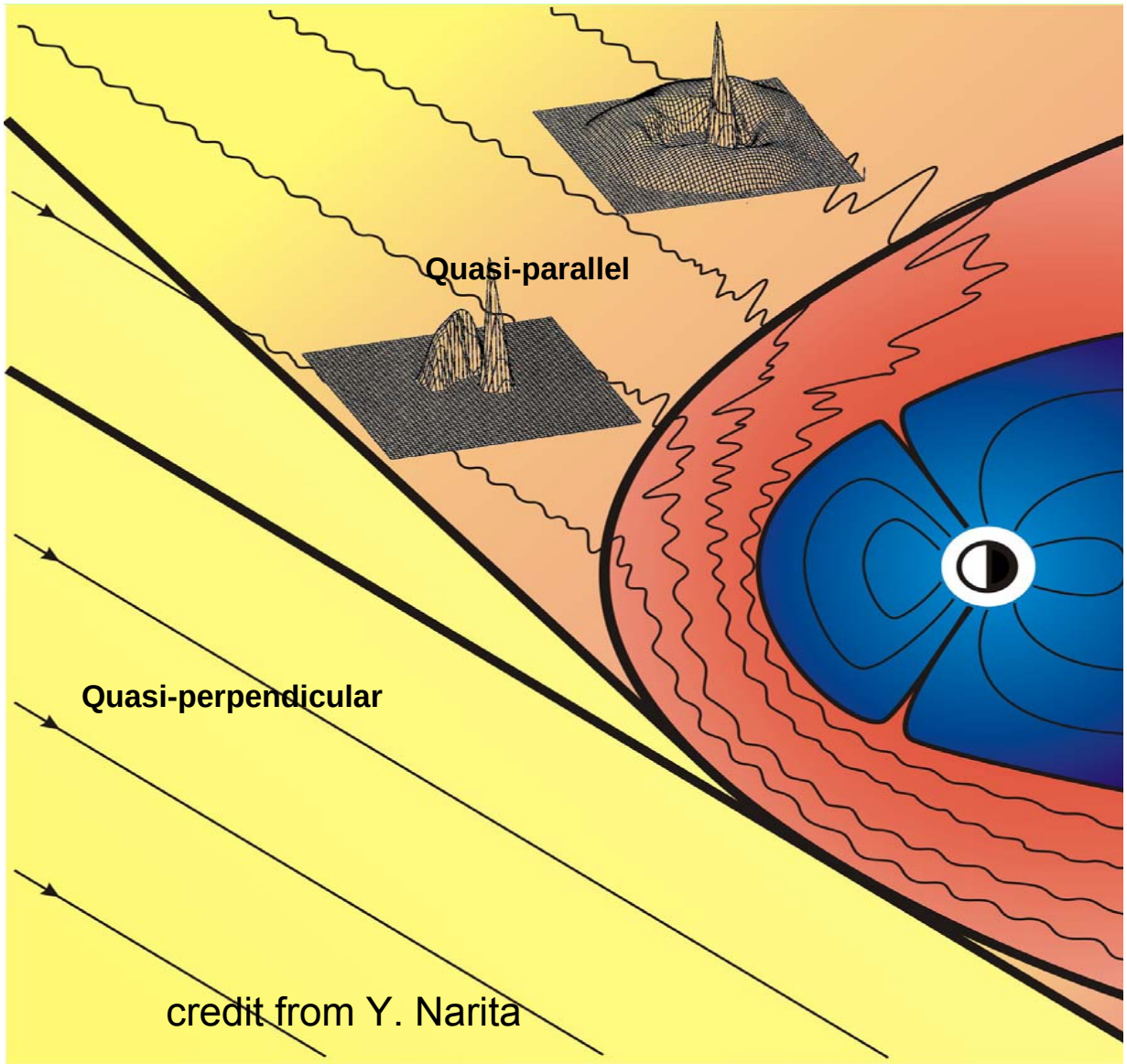

# Parallel and perpendicular shocks: magnetic field

The positions of the quasi-parallel and quasi-perpendicular shock regions move due to the change in the IMF direction.

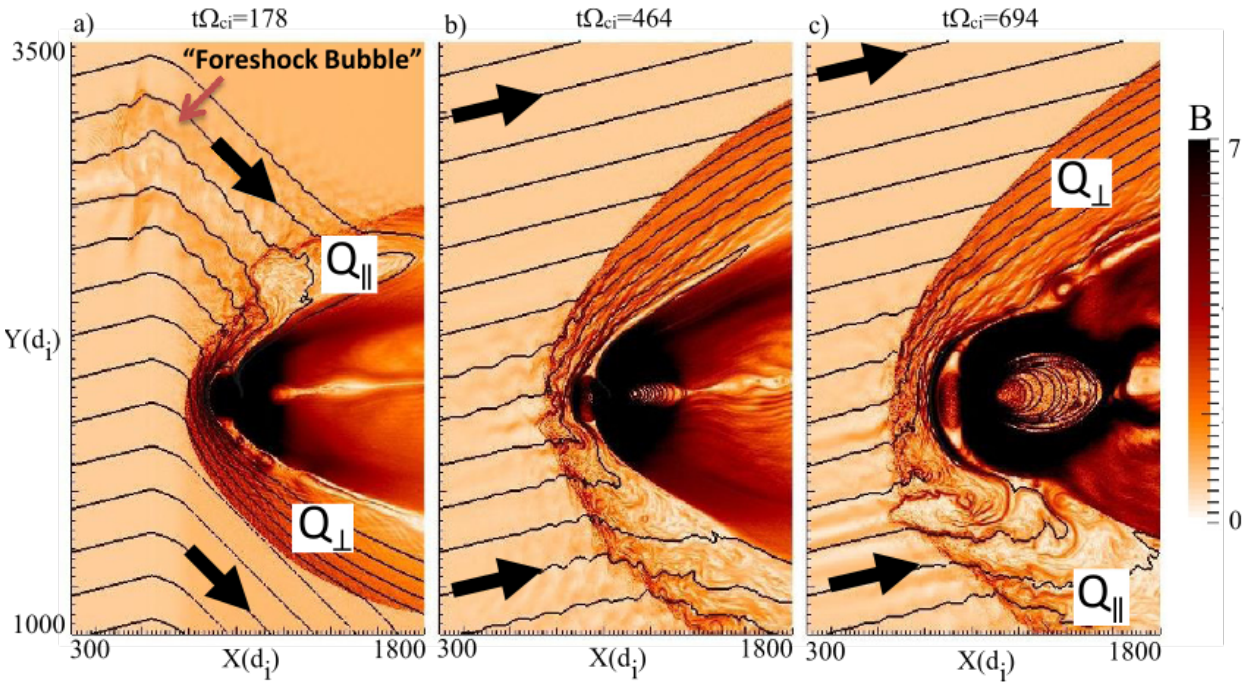


Karimabadi+14

# Quasi-parallel and quasi-perpendicular shocks: temperature

The enhanced heating in the quasi-parallel as compared to quasi-perpendicular magnetosheath is clearly evident.

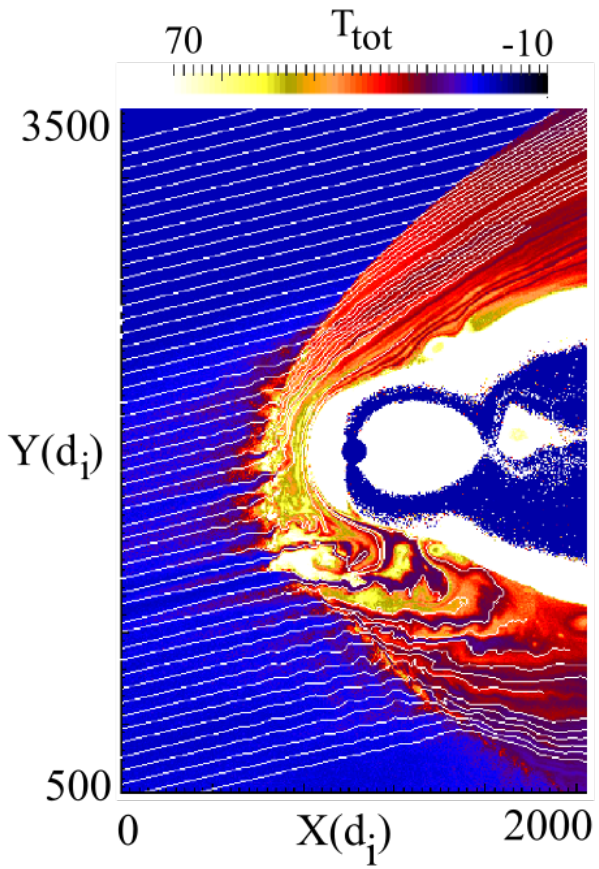


Karimabadi+14

# Tools to study bow shock

To study the solar wind-Earth interaction we have an excellent tool: mission CLUSTER

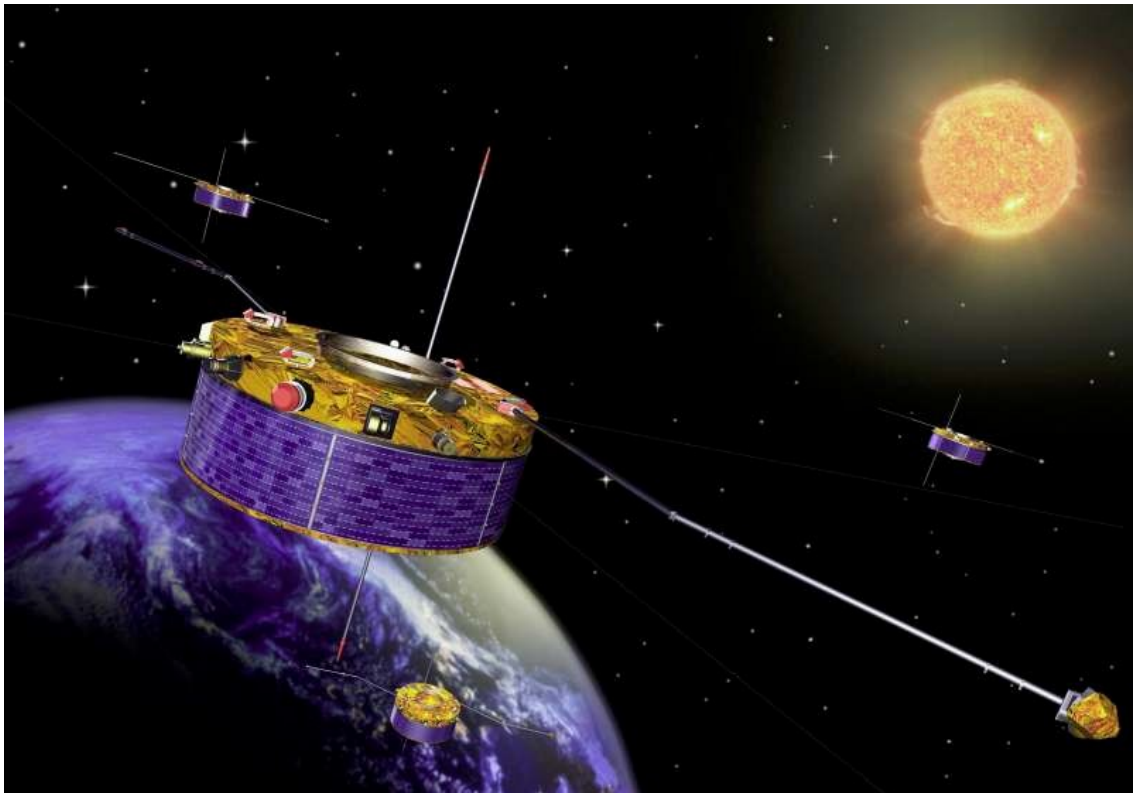

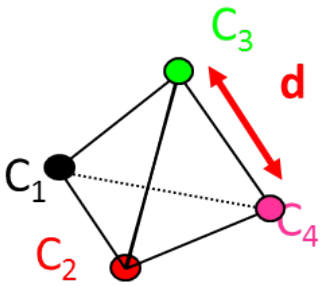

# Cluster orbits 2001–2012

"Orbits are traversing the regions of prime interest in the magnetosphere, both at high and low latitudes."

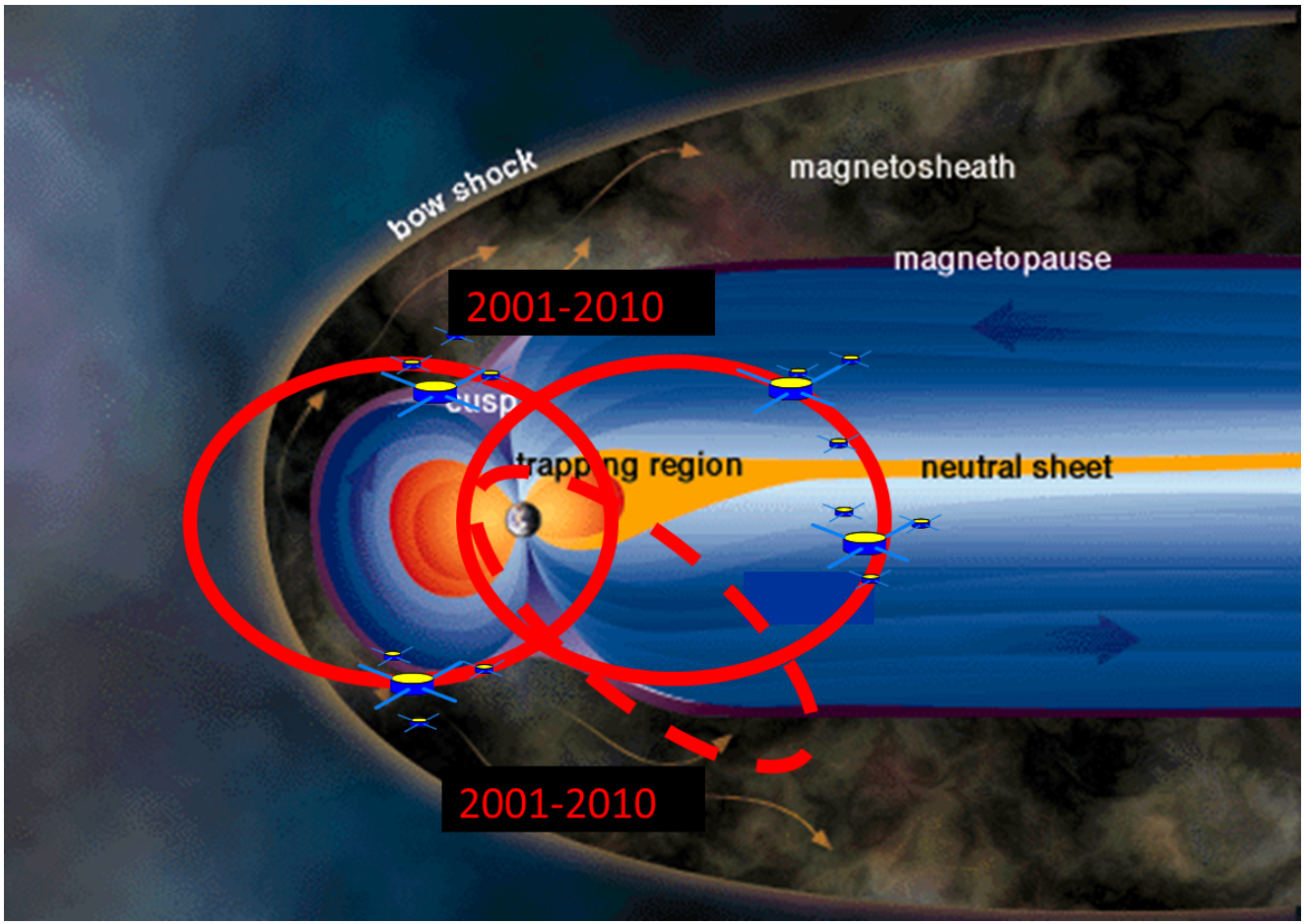

# Cluster separation

"The strategy governing the separation between four spacecraft of the cluster which is varied according to the most important scale sizes of the phenomena to be studied."

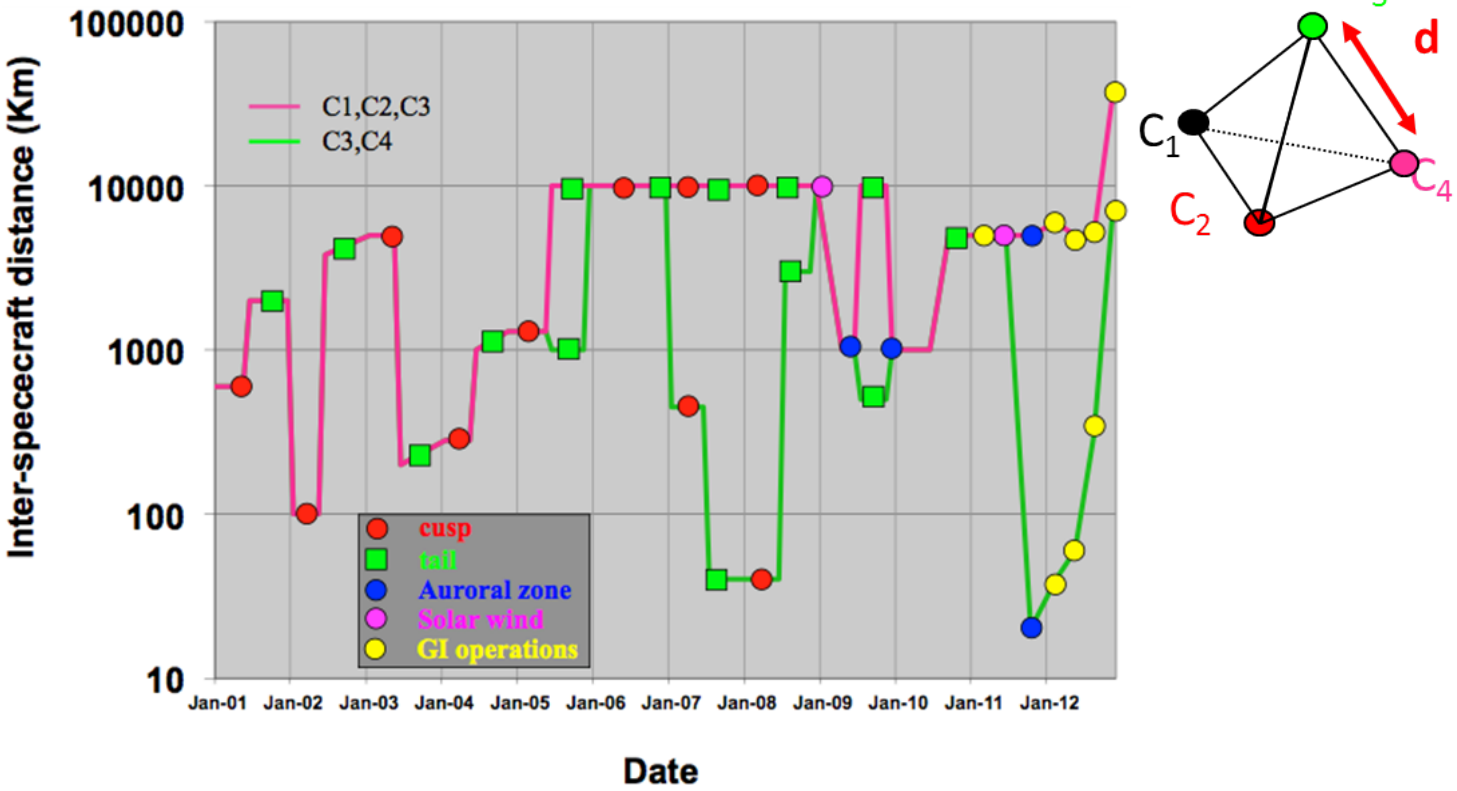

# Cluster Instruments

Each of the four spacecraft are equipped with a full complement of particle and field instruments.

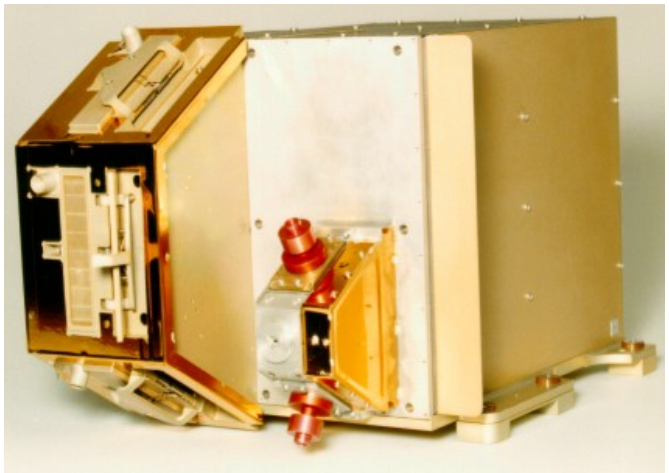

RAPID: ~30 keV – 1 MeV

CIS: ~0.01 keV – 35 keV

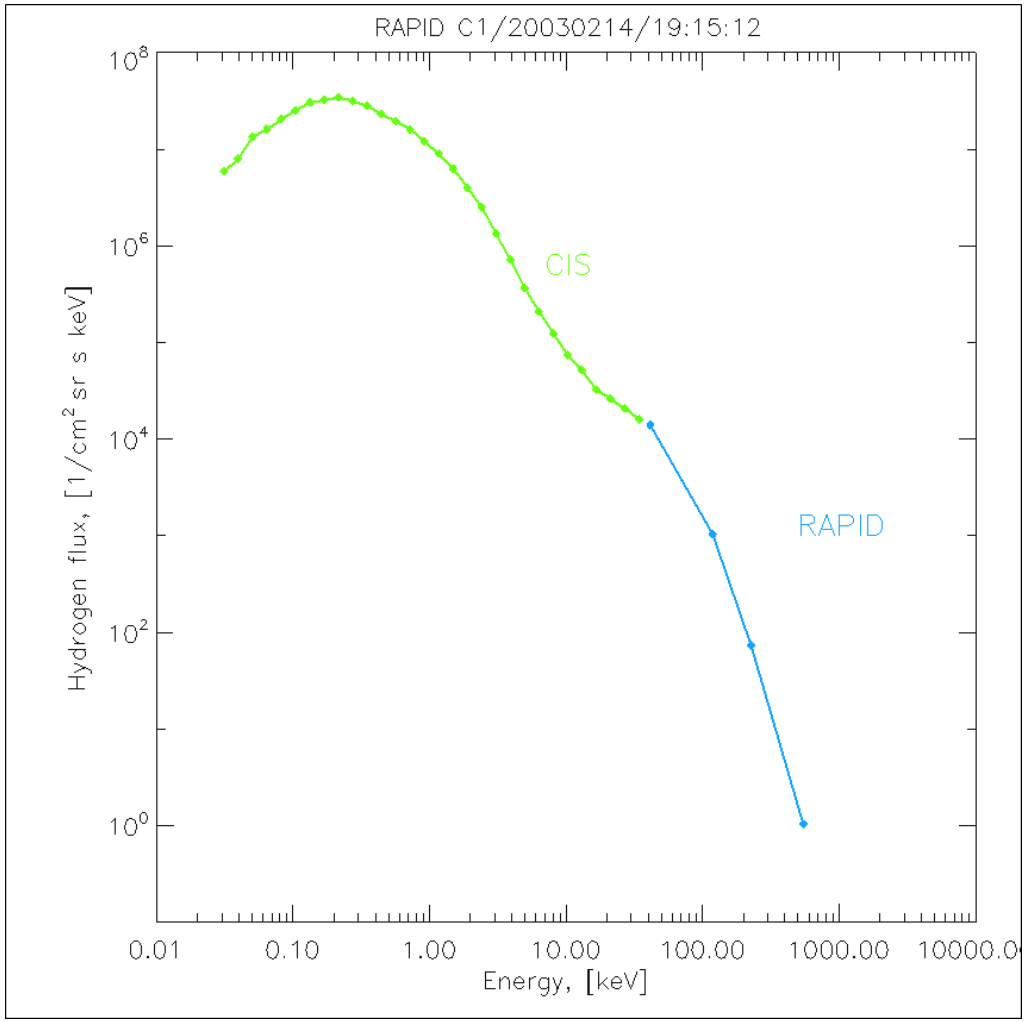

# Fluxgate Magnetometer (FGM)

- Each instrument consists of two triaxial fluxgate magnetometers and onboard Data-Processing Unit (DPU)
- The mass of each sensor is 290 g + 48 g for the thermal cover.
- The mass of the electronics box is 2060 g.
- The instrument power consumption in normal operations is 2460 mW.
- In order to minimise the magnetic background of the spacecraft, one of the magnetometer sensors is located at the end of 5.2 m radial boom, the other at 1.5 m inboard from the end of the boom.
- Different ranges from -64 to +64 nT with resolution of 7.8 $10^{-3}$ nT and from -65536 to +65528 nT with resolution of 8 nT
- Telemetry: 15.5 vector/second (Nominal mode) to 67.2 vector/second (Burst mode)

# Upstream region, parallel bow shock: example CME passage, solar maximum

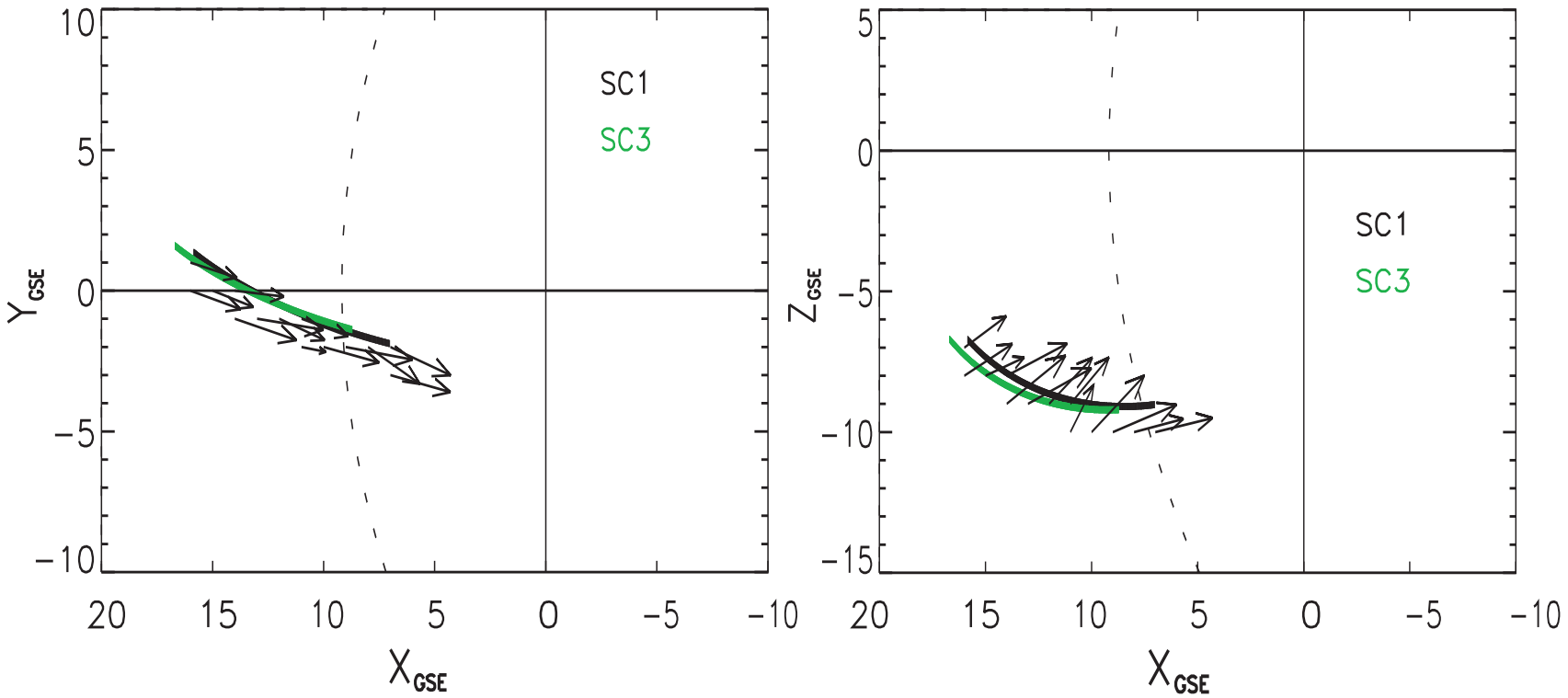


Kronberg et al., 2009

# Upstream region, parallel bow shock: example

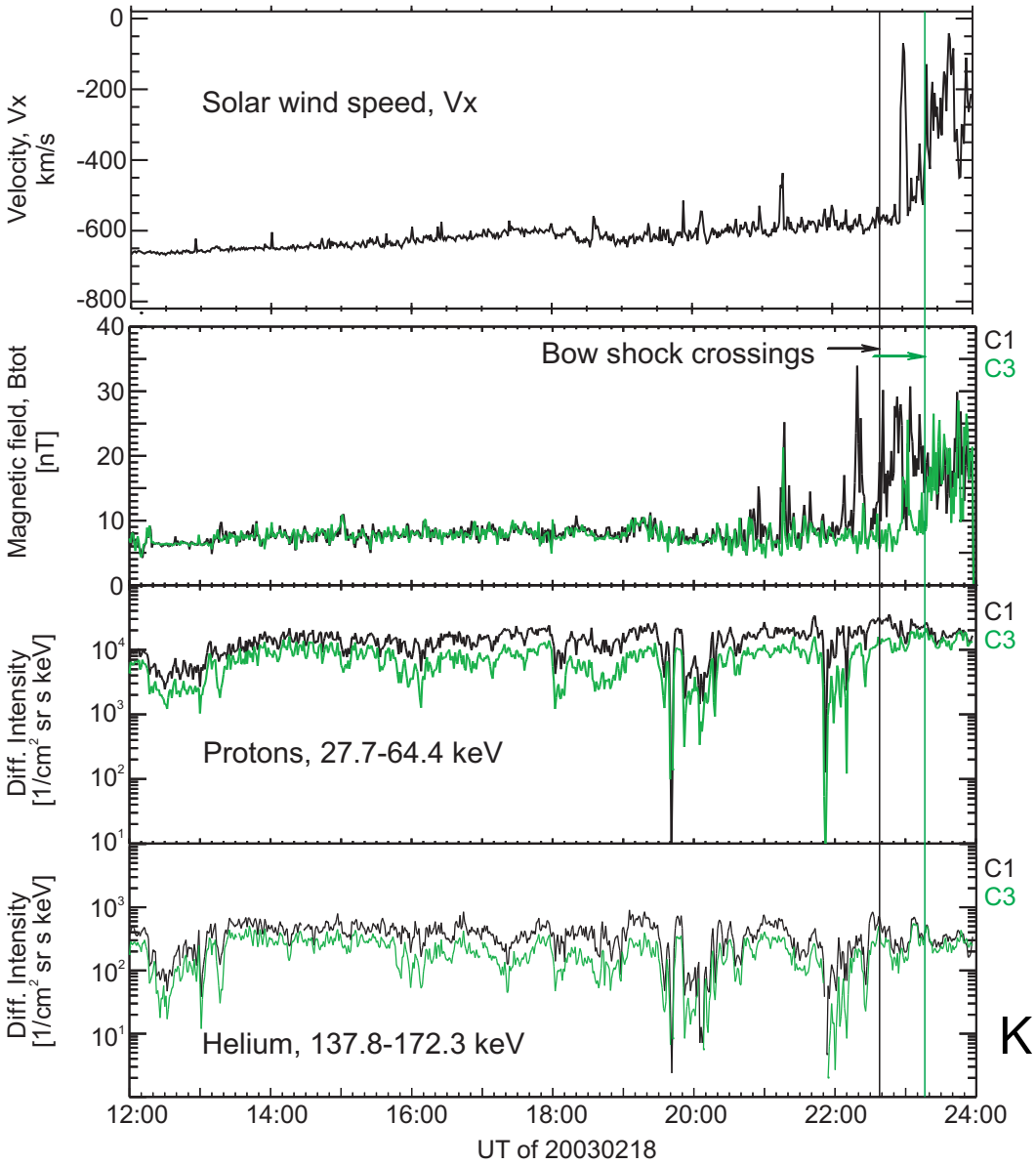


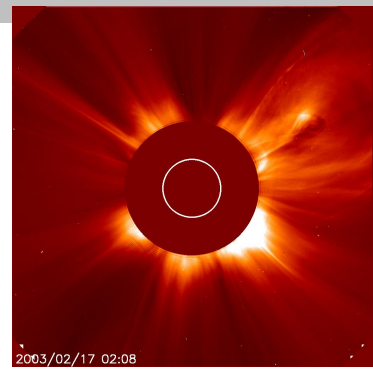


Kronberg et al., 2009

# Diffusive or first order Fermi acceleration

Credit: Treumann&Jaroschek

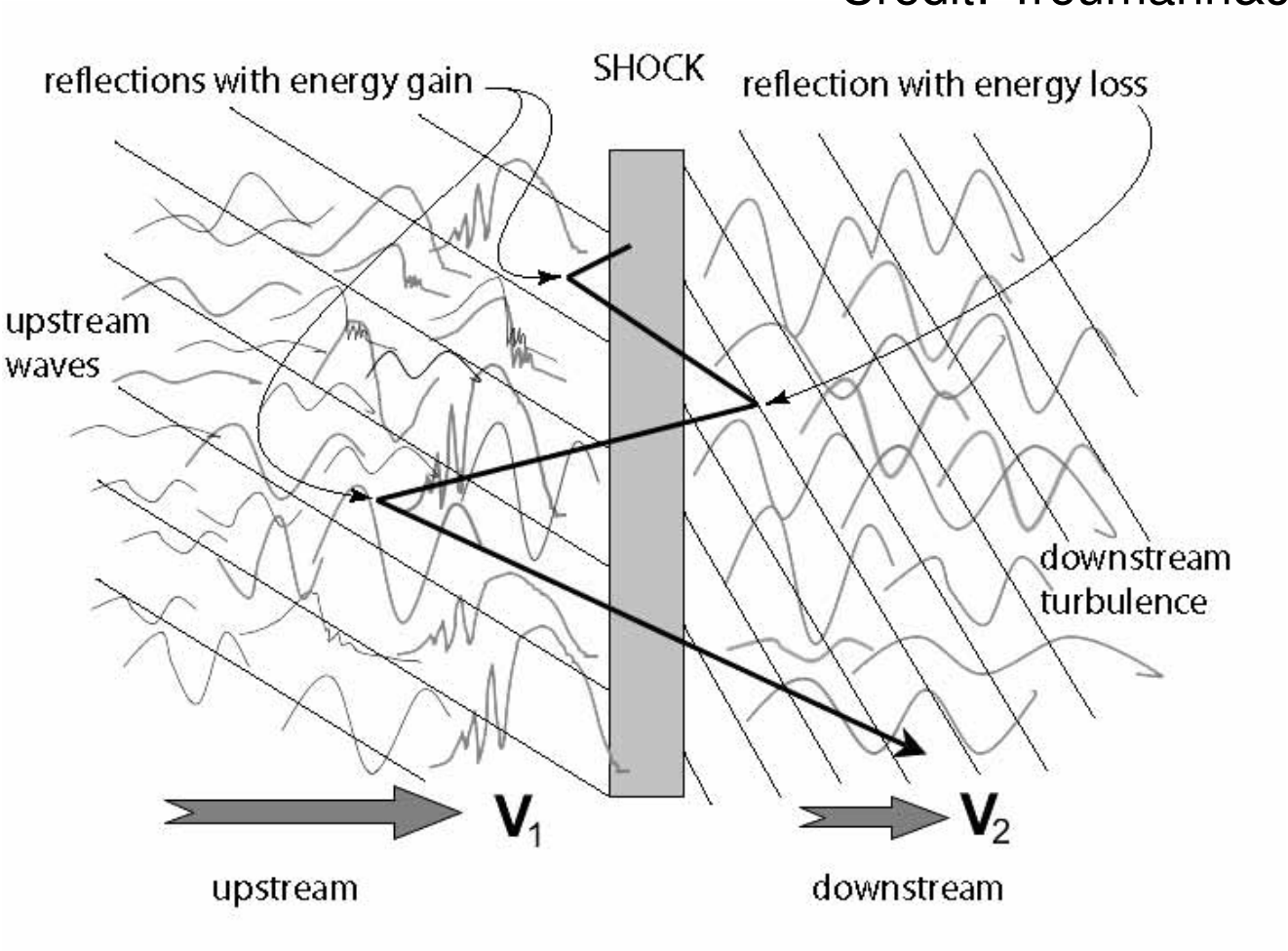


- Spatial gradient of density of upstream ions is expected to decrease exponentially with distance from the bow shock [e.g. Terasawa+81].

# Upstream region: acceleration at the bow shock
# CME passage, solar cycle maximum

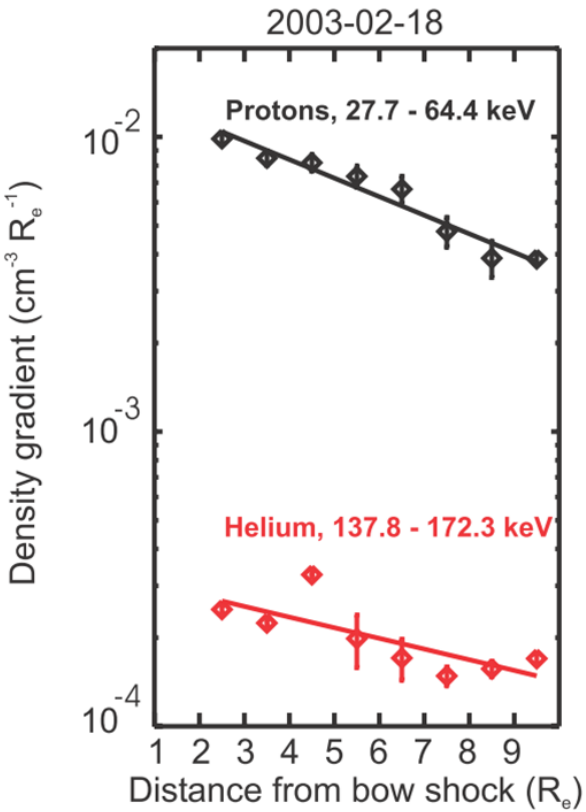


Kronberg+09

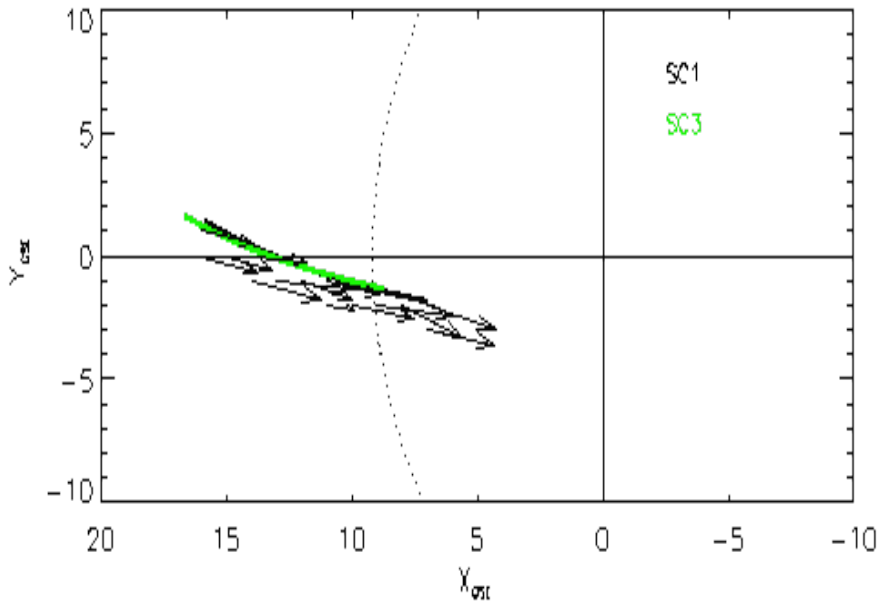


- Spatial gradient of the partial density of upstream ions is calculated.

# Upstream region: acceleration at the bow shock
# CME passage, solar cycle maximum

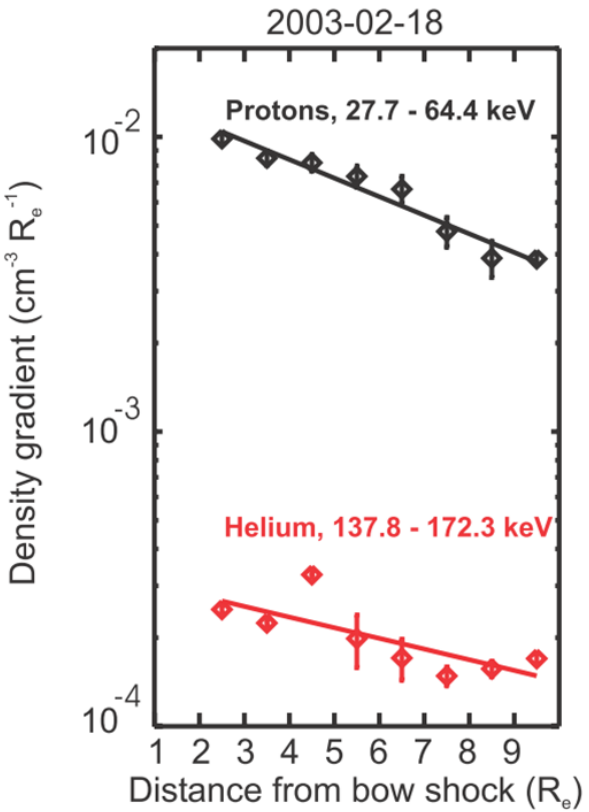


Kronberg+09

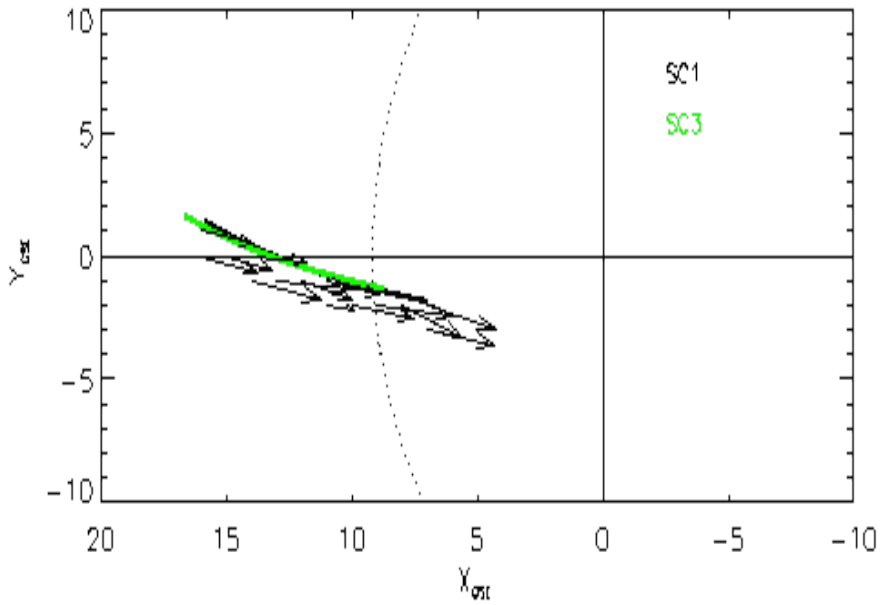


- Spatial gradient of the partial density of upstream ions is calculated.
- Scattering with waves and diffusive transport ⇒ gradients decrease exponentially with distance.

# Formation of shock between solar wind streams

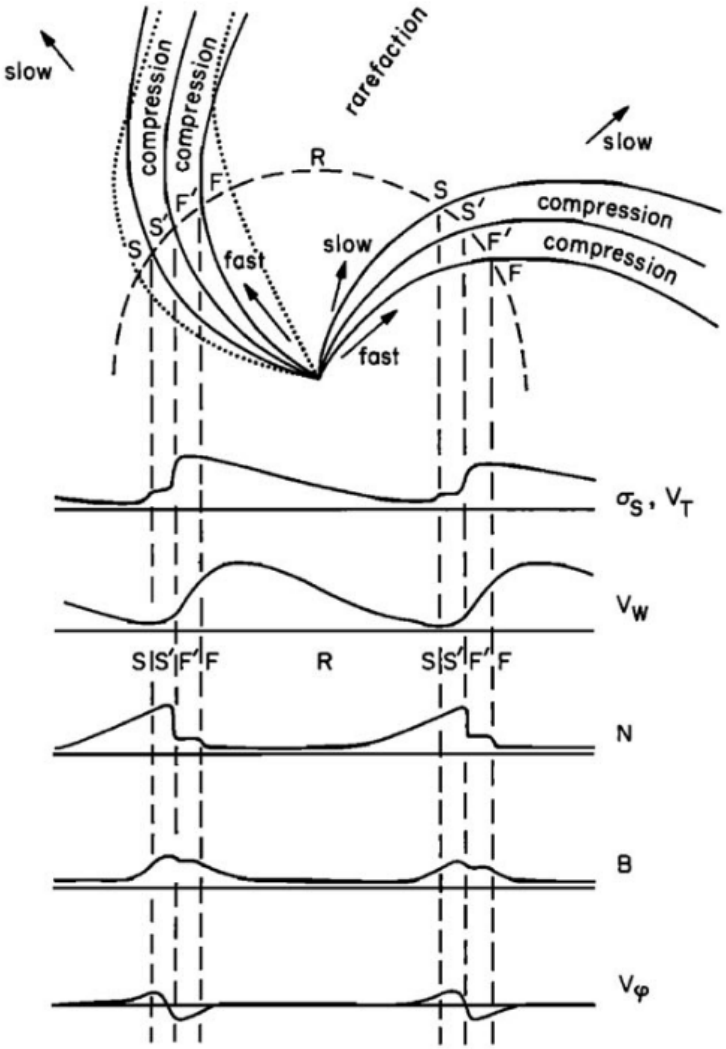


Richardson+18

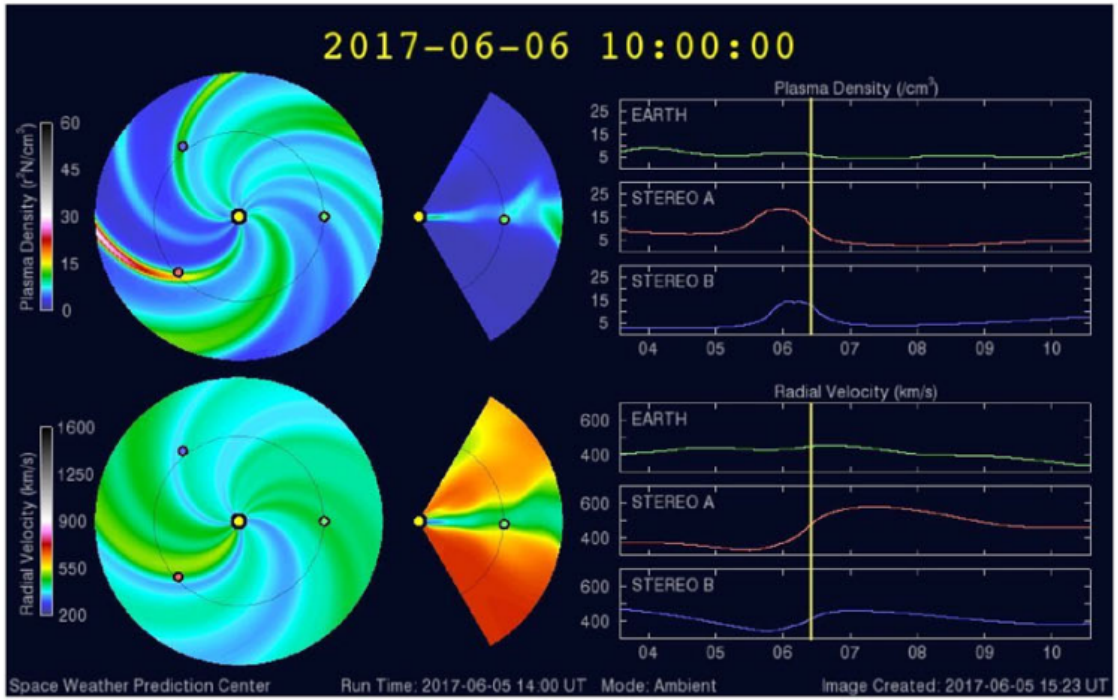

# Upstream region: CIR passage, solar cycle minimum

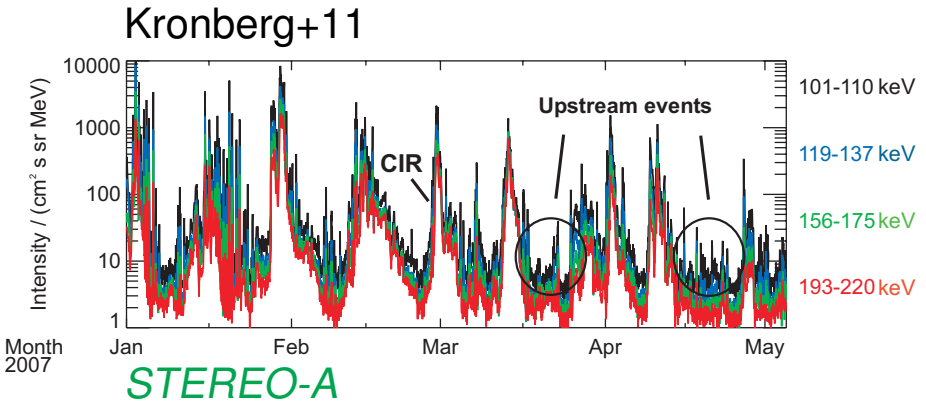


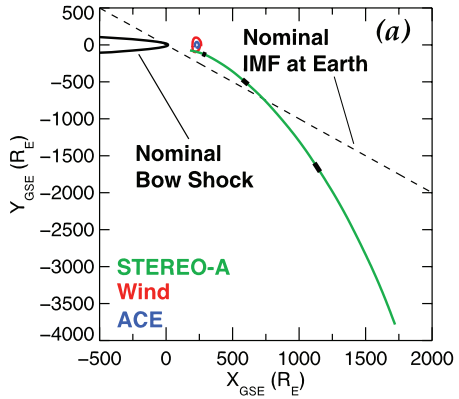


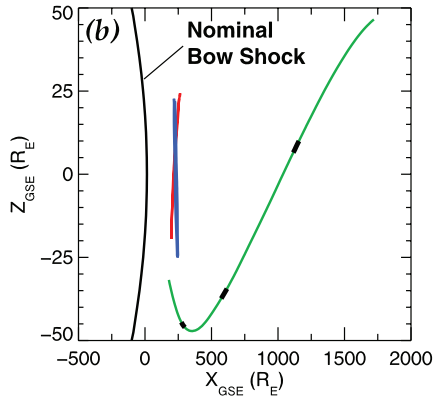


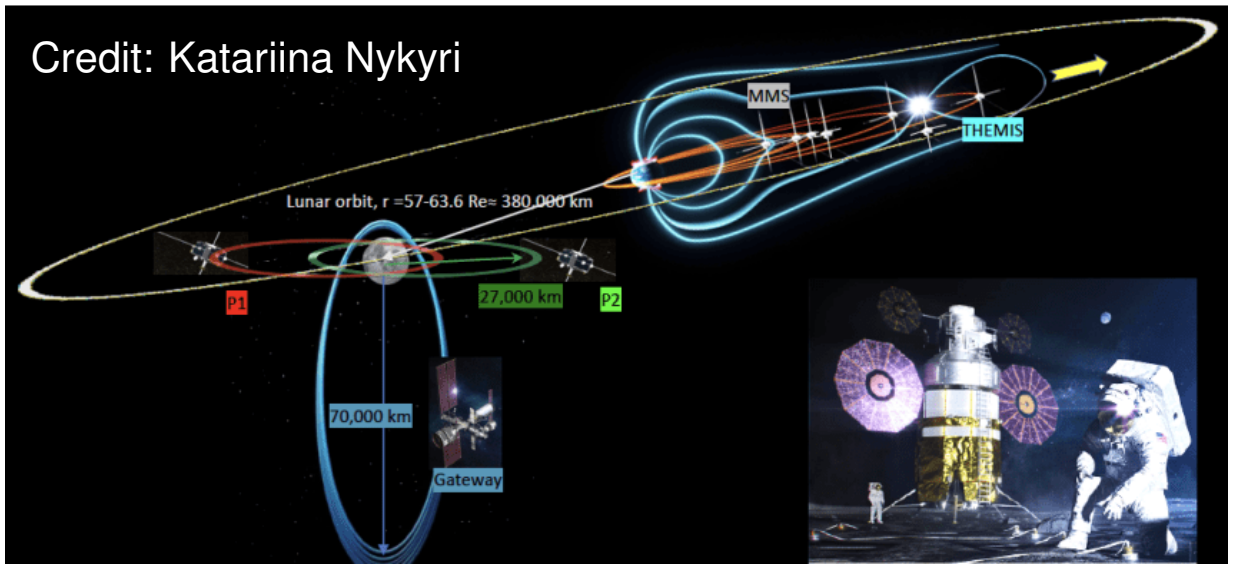


- Moon-exploration team will be affected by energetic particles in upstream region

# Shocks in the universe

Credit: N. Ganushkina, A. Spitkovsky

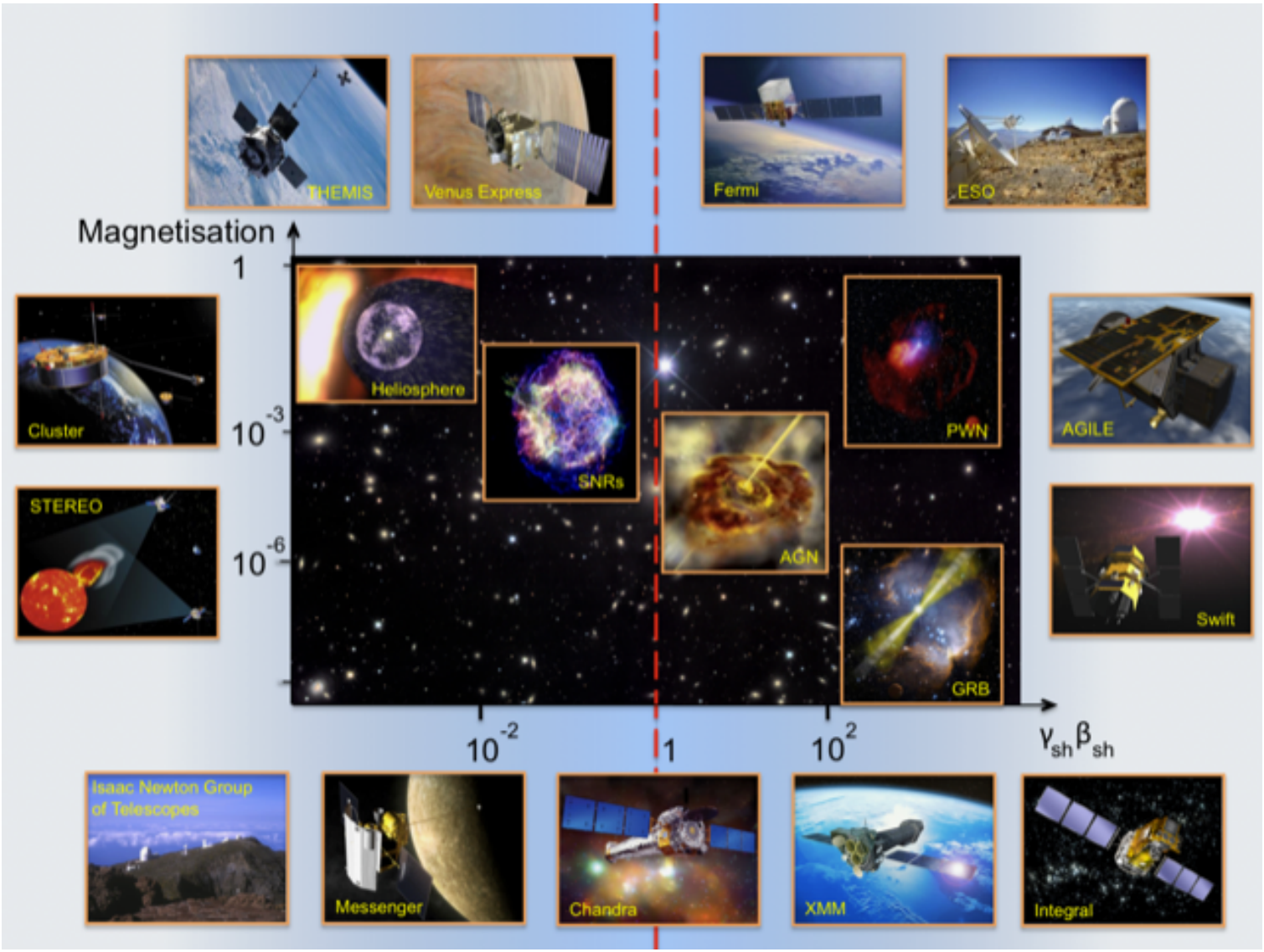

# Future applications?


# Summary

- Planetary shocks are complicated structures
- They lead to strong energization of plasma which can affect the satellites.
- Energetic particles can enter into the deepest lunar wake and raise the electric potential of the lunar surface (Nishino+17). This can affect the distribution of the dust on the lunar surface and, therefore, manned activities.

# Literature


- W. Baumjohann and R. Treumann, Basic Space Plasma Physics, 1996
- A. Brekke, Physics of the Upper Polar Atmosphere, 2013
- I. H. Cairns & J. G. Lyon, Magnetic field orientation effects on the standoff distance of Earth's bow shock, GRL, 23, 1996
- M. I. Desai et al., The spatial distribution of upstream ion events from the Earth's bow shock measured by ACE, Wind, and STEREO, JGR, V. 113, A08103, 2008
- H. Karimabadi, et al., The link between shocks, turbulence, and magnetic reconnection in collisionless plasmas, Physics of Plasmas, 21, 2014
- M. Kivelson and C. Russell, Introduction to Space Physics, 1995
- E. A. Kronberg, et al., Multipoint observations of ions in the 30-160 keV energy range upstream of the Earth's bow shock, JGR, 10.1029/2008JA013754, 2009
- E. A. Kronberg et al., On the origin of the energetic ion events measured upstream of the Earth's bow shock by STEREO, Cluster, and Geotail, JGR, 10.1029/2010JA015561, 2011
- M. N. Nishino et al., Kaguya observations of the lunar wake in the terrestrial foreshock: Surface potential change by bow-shock reflected ions, Icarus, doi: 10.1016/j.icarus.2017.04.005, 2017

# Literature


- F. Menk and C. Waters, Magnetoseismology: Ground-based remote sensing of Earth's magnetosphere, 2013
- M. Peredo et al., Three-dimensional position and shape of the bow shock and their variation with Alfvenic, sonic and magnetosonic Mach numbers and interplanetary magnetic field orientation, JGR, 100, 1995
- T. Terasawa, Energy spectrum of ions accelerated through Fermi process at the terrestrial bow shock, JGR, vol. 86, 1981
- R. A. Treumann & C. H. Jaroschek, Fundamentals of Non-relativistic Collisionless Shock Physics: V. Acceleration of Charged Particles, ARXIV [astro-ph], 2008